

7-2019

Second-order Dirac Superconductors and Magnetic Field Induced Majorana Hinge Modes

Sayed Ali Akbar Ghorashi

Xiang Hu

Taylor L. Hughes

Enrico Rossi

William & Mary, erossi@wm.edu

Follow this and additional works at: <https://scholarworks.wm.edu/aspubs>



Part of the [Physics Commons](#)

Recommended Citation

Akbar Ghorashi, Sayed Ali; Hu, Xiang; Hughes, Taylor L.; and Rossi, Enrico, Second-order Dirac Superconductors and Magnetic Field Induced Majorana Hinge Modes (2019). *Physical Review B*, 100(2). <https://doi.org/10.1103/PhysRevB.100.020509>

This Article is brought to you for free and open access by the Arts and Sciences at W&M ScholarWorks. It has been accepted for inclusion in Arts & Sciences Articles by an authorized administrator of W&M ScholarWorks. For more information, please contact scholarworks@wm.edu.

Second-order Dirac superconductors and magnetic field induced Majorana hinge modesSayed Ali Akbar Ghorashi,^{1,*} Xiang Hu,¹ Taylor L. Hughes,² and Enrico Rossi¹¹*Department of Physics, William & Mary, Williamsburg, Virginia 23187, USA*²*Department of Physics and Institute for Condensed Matter Theory, University of Illinois at Urbana-Champaign, Illinois 61801, USA*

(Received 28 January 2019; revised manuscript received 22 April 2019; published 31 July 2019)

We identify three-dimensional higher-order superconductors characterized by the coexistence of one-dimensional Majorana hinge states and gapless surface states. We show how such superconductors can be obtained starting from the model of a spinful quadrupolar semimetal with two orbitals and adding an s -wave superconducting pairing term. By considering all the possible s -wave pairings satisfying Fermi-Dirac statistics we obtain six different superconducting models. We find that for two of these models a flat band of hinge Majorana states coexist with surface states, and that these models have a nonvanishing quadrupolelike topological invariant. Two of the other models, in the presence of a Zeeman term, exhibit helical and dispersive hinge states localized only at two of the four hinges. We find that these states are protected by combinations of rotation and mirror symmetries, and that the pair of corners exhibiting hinge states switches upon changing the sign of the Zeeman term. Furthermore, we show that these states can be localized to a single hinge with suitable perturbations. The remaining two models retain gapless bulk and surface states that spectroscopically obscure any possible hinge states.

DOI: [10.1103/PhysRevB.100.020509](https://doi.org/10.1103/PhysRevB.100.020509)

The modern theory of polarization for crystalline insulators [1] has revealed that in crystals a dipole moment can be expressed in terms of Berry phases, and that a finite dipole necessarily implies the presence of boundary charges. The presence of nontrivial Berry phases and boundary states are the hallmarks of topological systems [2], and indeed it is now clear that there is a strong connection between the theory of topological insulators (TIs) and systems with quantized dipole moments [3–5]. This connection has led to the realization that the extension of the modern theory of polarization to higher multipole moments allows the identification of new classes of topological crystalline insulators [6,7], termed “higher-order” TIs (HOTIs). Within this framework, a higher-order multipole TI of order m has a quantized nonzero electric m th pole in the bulk (with $m = 1$ for a dipole, $m = 2$ for a quadrupole,...) and localized charges at its $(d - m)$ -dimensional boundaries, d being the insulator’s spatial dimension. Since the work of Refs. [6,7], many proposals of HOTIs of various types have been presented [8–12]. Higher-order topological insulating phases have been realized in metamaterial arrays [13–15] and phononic systems [16], and it has been proposed that bismuth [10], strained SnTe [8], and some two-dimensional (2D) transition metal dichalcogenides [17] are second-order TIs. In addition, there has been exciting new work on higher-order topological superconductors (HOTSCs) and topological semimetals (HOTSMs) [9,17–23,25–31].

In this work we identify a class of higher-order topological superconductors: *second-order Dirac superconductors* (Fig. 1). Such three-dimensional (3D) higher-order topological superconductors exhibit the unique property to have both topologically protected Dirac cones for states at the

surface (d-1 boundary) and topologically protected dispersionless Majorana states at the hinges (d-2 boundary). The hinge states can be interpreted as Majorana arcs joining the surface Dirac points. We explicitly show that this unique configuration of surface and hinge states is associated with a topological invariant that can be interpreted as the generalization to the superconducting case of the quadrupole moment. This model can provide a platform to study the interplay of the bulk, surface, and hinge states on an equal footing which can significantly help toward understanding the transport properties of systems with higher-order topology. In addition, we identify 3D superconducting systems that can be driven into a higher-order topological state, exhibiting dispersive helical Majorana states at the hinges, simply via the application of an external magnetic field. Interestingly, we find that the hinges are localized at only two of the four hinges (see [23] and [24] for insulating examples of states localized at two corners). Furthermore, the pairs of corners where the Majorana modes are located can be selected by changing the sign of the magnetic field. We also show that by breaking diagonal/antidiagonal mirror symmetries, it is possible to drive the system into a unique topological state in which Majorana states are present only at one of the hinges.

We start by considering a model for a topological quadrupolar semimetal constructed from layers of 2D quadrupolar topological insulators (TIs) [32]. Schematically, the unit cell for the tight-binding model for the 2D quadrupolar insulator layer is illustrated in Fig. 1(c). For each cell we have two orbitals (c, d) and a spin-1/2 degree of freedom, represented by the four black dots in Fig. 1(c). Let γ_i ($i = x, y$) be the intracell hopping amplitudes [red lines in Fig. 1(c)] and λ_i the intercell hopping [blue lines in Fig. 1(c)]. Hopping processes represented by dotted lines have a phase that is opposite to that of the hopping processes represented by solid

*sghorashi@wm.edu

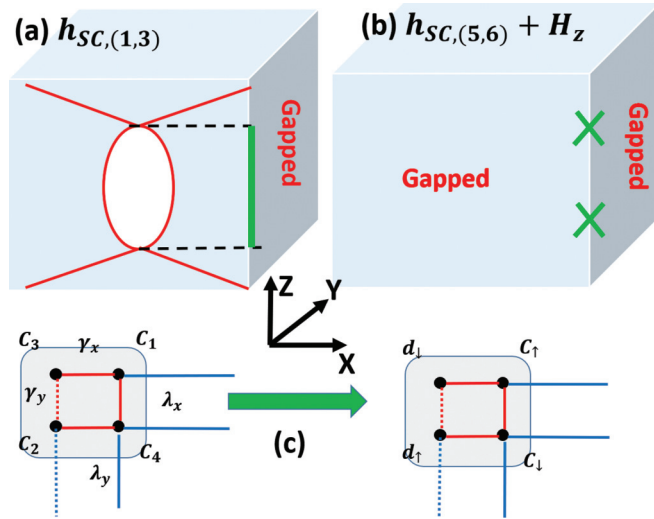


FIG. 1. Summary illustration of the models with hinge modes studied in this work. (a) Model $h_{SC,1}$ (rotate by C_4 for model $h_{SC,3}$). (b) Models $h_{SC,5}$, $h_{SC,6}$ with magnetic field (Zeeman term H_z) in the z direction. Red lines represent surface states for $k_{x,y} = 0$ cuts. Green lines represent flat-band hinge states; green crosses represent dispersing hinge nodes. (c) The unit cell convention used to convert between spinless and spinful versions of HOTI and HOTSM.

lines. Depending on the choice of interlayer tunneling terms between 2D layers of quadrupolar TIs we obtain different Hamiltonians, H , for the resulting 3D system. In momentum space we have $H_{SM} = \sum_{\mathbf{k}} \psi_{\mathbf{k}}^\dagger h_{SM}(\mathbf{k}) \psi_{\mathbf{k}}$, where $\psi_{\mathbf{k}}^T$ is the spinor $(c_{\mathbf{k}\uparrow}, d_{\mathbf{k}\uparrow}, d_{\mathbf{k}\downarrow}, c_{\mathbf{k}\downarrow})$, formed by the annihilation operators $c_{\mathbf{k}\alpha}, d_{\mathbf{k}\alpha}$, for an electron in orbitals c, d , with spin α and momentum \mathbf{k} , and h_{SM} is a 4×4 Bloch Hamiltonian matrix of the general form:

$$h_{SM}(\mathbf{k}) = [\gamma_x + \chi_x(k_z) + \lambda_x \cos(k_x)]\Gamma_4 + \lambda_x \sin(k_x)\Gamma_3 \\ + [\gamma_y + \chi_y(k_z) + \lambda_y \cos(k_y)]\Gamma_2 + \lambda_y \sin(k_y)\Gamma_1. \quad (1)$$

In Eq. (1) all the lattice constants are taken to be 1, $\chi_i(k_z)$ ($i = x, y$) are periodic functions of k_z with forms fixed by the interlayer tunneling terms, and $\{\Gamma_\alpha\}$ are the 4×4 matrices given by the direct product of 2×2 Pauli matrices σ_i, κ_i in spin and orbital space, respectively: $\Gamma_0 = \sigma_3 \kappa_0$, $\Gamma_i = -\sigma_2 \kappa_i$, $\Gamma_4 = \sigma_1 \kappa_0$. In the remainder we assume $\chi_i(k_z), \gamma_i, \lambda_i$ to be independent of the in-plane direction (x or y) such that the normal state topological quadrupolar semimetal has C_4 symmetry. To be explicit we will set $\lambda_i = \lambda$ and use it as our unit of energy with $\lambda = 1$. We then set $\chi_i(k_z) = \cos(k_z)/2$, and $\gamma_i = \gamma = -3/4$. With this choice of parametrization, $h_{SM}(\mathbf{k})$ has fixed k_z “momentum slices” with a nonvanishing quantized quadrupole moment for $\cos(k_z) < -1/2$, and vanishing quadrupole for $\cos(k_z) > -1/2$. As a consequence, the bulk bands are semimetallic with fourfold degenerate nodes at the locations $k_z^{(c)}$ where the quadrupole changes, i.e., $\cos(k_z^{(c)}) = -1/2$ [32]. It is important to point out that any HOTSM with a well-defined nontrivial quadrupole moment and C_4 and mirror symmetries should lead, in the presence of s -wave superconducting pairing, to results qualitatively similar to the one that we present below. The presence of the C_4 and mirror

TABLE I. The pairings for the six different models discussed in this work. Columns 2–4 show the representation of the pairing term and of the symmetry operators for each model. $m_x = \sigma_1 \kappa_3$, $m_y = \sigma_1 \kappa_1$, $\hat{r}_4 = \frac{i}{2}(\sigma_1 + i\sigma_2)\kappa_2 + \frac{1}{2}(\sigma_1 - i\sigma_2)\kappa_0$. Column 6 shows the pairing structure: inter/intra and S/T are short for inter/intra orbital and spin singlet/triplet, respectively. Column 7 shows whether the model is a HOTSC: models with an “*” in parentheses denotes the existence of HOTSC in the presence of magnetic field.

Model	Λ_i	\mathcal{M}_x	\mathcal{M}_y	C_4	Structure	HOTSC
$h_{SC,1}$	$\sigma_1 \kappa_2$	$\tau_3 m_x$	$\tau_3 m_y$		intra-S	✓
$h_{SC,2}$	$\sigma_2 \kappa_1$	$\tau_0 m_x$	$\tau_3 m_y$		intra-S	✓
$h_{SC,3}$	$\sigma_2 \kappa_0$	$\tau_3 m_x$	$\tau_3 m_y$		inter-S	✓
$h_{SC,4}$	$\sigma_2 \kappa_3$	$\tau_3 m_x$	$\tau_0 m_y$		inter-T	✓
$h_{SC,5}$	$\sigma_0 \kappa_2$	$\tau_3 m_x$	$\tau_3 m_y$	$\tau_0 \hat{r}_4$	inter-S	–(✓*)
$h_{SC,6}$	$\sigma_3 \kappa_2$	$\tau_0 m_x$	$\tau_0 m_y$	$\tau_3 \hat{r}_4$	intra-T	–(✓*)

symmetries is important, as we will show, to be able to “tune” the hinge states via external magnetic fields.

The most general mean-field Hamiltonian describing a superconducting state for our system is given by $H_{SC} = \sum_{\mathbf{k}} \Psi_{\mathbf{k}}^\dagger h_{SC}(\mathbf{k}) \Psi_{\mathbf{k}}$ where $\Psi_{\mathbf{k}}^T = (\psi_{\mathbf{k}}, \psi_{-\mathbf{k}}^\dagger)$ is the spinor in Nambu space and $h_{SC}(\mathbf{k}) = \tau_3 [h_{SM}(\mathbf{k}) - \mu] + \Delta_0^{(ij)}(\mathbf{k}) \tau_2 \sigma_i \kappa_j$, where μ is the chemical potential, $\Delta_0^{(ij)}(\mathbf{k})$ the superconducting pairing strength in the (ij) spin-orbital channel, and $\{\tau_i\}$ are the Pauli matrices in Nambu space. Restricting the superconducting pairing to be s -wave, i.e., $\Delta_0^{(ij)}(\mathbf{k}) = \text{const} = \Delta_0$, we obtain

$$h_{SC,i} = \tau_3 [h_{SM}(\mathbf{k}) - \mu] - \Delta_0 \tau_2 \Lambda_i, \quad (2)$$

where Λ_i is a 4×4 matrix, independent of \mathbf{k} , that determines the structure of the superconducting pairing in orbital and spin space. The requirement that the pairing term satisfies Fermi-Dirac statistics implies that there are only six possible pairing matrices Λ_i , listed in the second column of Table I (see, e.g., [33]). As a consequence, starting from h_{SM} , we can obtain six distinct s -wave superconducting states.

The normal state already has broken time-reversal symmetry ($T^2 = -1$); when the superconducting pairing is added these superconductors belong to symmetry class D [2]. We note that our model has a pseudo-chiral symmetry but its presence is not required for our results. All the models have mirror symmetries $\mathcal{M}_x, \mathcal{M}_y$, and \mathcal{M}_z , and therefore overall inversion symmetry $\mathcal{I} = \mathcal{M}_x \mathcal{M}_y \mathcal{M}_z$. The representation matrices for the \mathcal{M}_x and \mathcal{M}_y mirror symmetries are shown in Table I, and the matrix for \mathcal{M}_z is the identity matrix. Models $h_{SC,5}, h_{SC,6}$, retain C_4 symmetry in the superconducting state with representation matrices given in Table I.

Let us consider the quasiparticle spectra in the weak pairing limit $\Delta_0 < \mu$. Explicitly, we choose $\mu = 1$, $\Delta_0 = 0.5$ and find that models $h_{SC,1}, h_{SC,3}, h_{SC,6}$ are fully gapped in the bulk by the pairing term while $h_{SC,2}, h_{SC,4}, h_{SC,5}$ are gapless [see Supplemental Material (SM) [34]]. Model $h_{SC,2}$ ($h_{SC,4}$) has gapless, bulk, quasiparticle states forming a nodal line/loop in the $k_x - k_z$ ($k_y - k_z$) plane, and model h_5 has four nodes in the $k_x - k_y$ plane at k_z values away from any high-symmetry points. We see that models $h_{SC,1}$ and $h_{SC,3}$ have the same symmetry, the same representation for \mathcal{M}_x and

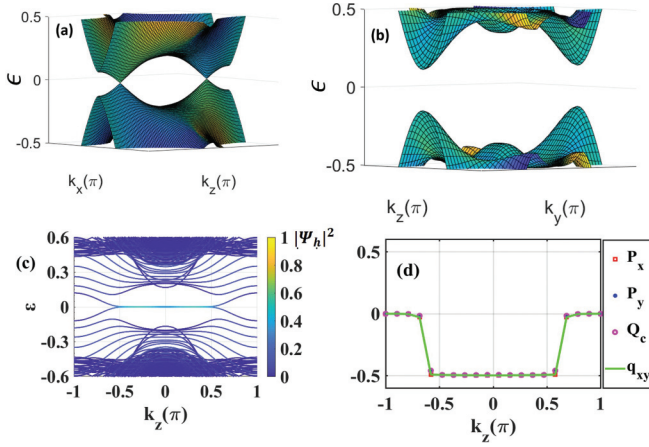


FIG. 2. The surface states of $h_{SC,1}$ in (a) k_x - k_z and (b) k_y - k_z planes. (c) shows the Majorana hinges arc states in the k_z direction. (d) P_x , P_y , Q_c and q_{xy} versus k_z .

\mathcal{M}_y , and have the same bulk spectra. Thus, they will have the same essential properties for our study, and henceforth we only consider $h_{SC,1}$. Additionally, models $h_{SC,2}$ and $h_{SC,4}$ are related by a unitary transformation and a C_4 rotation around the z axis so we will only consider $h_{SC,2}$ from now on. While we have focused on particular values of μ and Δ_0 , the results do not change qualitatively as long as $\Delta_0 < \mu$, as is appropriate for the weak-pairing limit.

We start by considering model $h_{SC,1}$. The pairing breaks C_4 symmetry, while retaining mirror symmetries, so the bulk are completely gapped [6] (see SM [34] for more details). However, we find that the surfaces $S_{y,\pm}$, perpendicular to the y axis, exhibit two gapless nodes per surface [Fig. 2(a)], whereas the ones perpendicular to the x axis, $S_{x,\pm}$, are completely gapped [Fig. 2(b)]. We then obtain the bands for the hinges and find, as shown in Fig. 2(c), that dispersionless hinge Majorana states are present at the four corners of the xy plane for values of k_z between the two gapless nodes on the S_y surface. In Fig. 2(c) and all the other plots showing the spectrum of hinge states, the color used for each point of the spectrum denotes the magnitude of the square of the corresponding eigenstate at the hinges $|\Psi_h|^2$. These states are reminiscent of the flat bands that appear between the nodes, and at the edges, of a 2D Dirac semimetal.

The structure of the spectrum and symmetry is similar to that of the quadrupolar semimetal obtained in Ref. [32] when $\gamma_i(k_z) \equiv \gamma_i + \chi(k_z)$ [$i = (x, y)$] follow what in Ref. [32] is referred to as path 2, and suggests that the presence of the boundary states, the hinge states in particular, might be due to a second-order topological invariant. To confirm it, we calculated (for details, see SM [34]) the superconducting analog of the quadrupole moment $q_{xy}(k_z)$ for each k_z slice. We have $q_{xy}(k_z) \equiv [P_x(k_z) + P_y(k_z) - Q_c(k_z)] \bmod 1$ [6] where $P_x(k_z)$, $P_y(k_z)$ are the surface polarizations in the x and y directions, respectively, and $Q_c(k_z)$ is the corner charge which takes values $1/2, (0) \bmod 1$, if hinge states are present (absent).

Figure 2(d) shows that $P_x(k_z)$, $P_y(k_z)$ are quantized, and that they take the nontrivial value $-1/2$ for k_z in the interval between the two gapless nodes of the surface states on S_y , the same range of k_z for which we have hinge states. As a

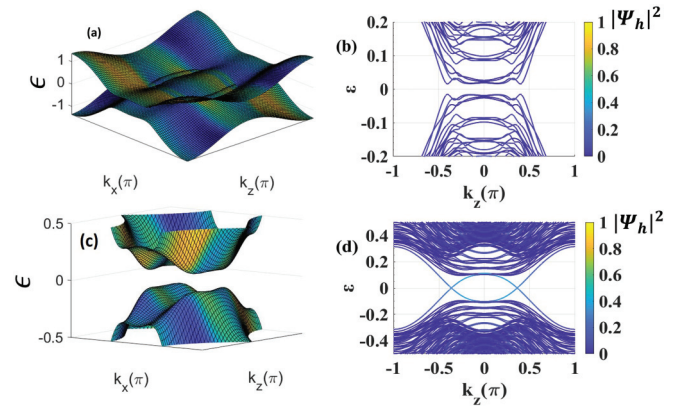


FIG. 3. Model $h_{SC,5}$: Surface states (a) in the k_x - k_z plane, and hinge states (b) along k_z , when $J_z = 0$, (c) and (d), same as (a) and (b), respectively, for the case when $J_z = 0.4$.

consequence, we find that for values of k_z between the two surface nodes, $q_{xy}(k_z)$ is also nontrivial and therefore that the hinge states in model $h_{SC,1}$ are topologically protected and can be captured by a second-order, quadrupolelike, topological invariant. Interestingly, we find that the presence of the gapless nodes on the surface, and of the hinge states, is not affected by perturbations that break both mirror symmetries, and thus the hinge states are perturbatively stable when the Bogoliubov–de Gennes particle-hole symmetry is maintained even when the mirror symmetry is broken (see SM [34]). Due to the presence of Dirac nodes in the band structure of the surface states, and the finite value of the quadrupolelike invariant we term superconductors like the one described by model $h_{SC,1}$ (and $h_{SC,3}$) as *second-order Dirac superconductors*. This is one of the main results of this work.

For models $h_{SC,2,4}$ the gapless nature of the bulk and surface states leads to obscured hinge modes (see Fig. 2 in SM [34]).

Models $h_{SC,5}$ and $h_{SC,6}$ differ from the previous models in that, in addition to the mirror symmetries \mathcal{M}_x and \mathcal{M}_y , they retain the C_4 symmetry of the original semimetal. As mentioned, model $h_{SC,5}$ has nodal points in the bulk quasiparticle spectrum, while $h_{SC,6}$ is fully gapped in the bulk (see SM [34]). We find that both models have gapless surface states but of different nature. Due to the C_4 symmetry, we only show the results for the surface states $S_{y,\pm}$. The surface bands of model $h_{SC,5}$ exhibit two nodal loops [see Fig. 3(a)], whereas the surface bands of model $h_{SC,6}$ exhibit a nodal line at $k_x = 0$ for the S_y surface states ($k_y = 0$ for the S_x surface states), Fig. 4(a). Figures 3(b) and 4(b) show the bands for the hinges for models $h_{SC,5}$ and $h_{SC,6}$ and we see that there are no interesting localized hinge modes present.

However, an external magnetic field can perturb these systems to generate hinge modes. Let us apply a uniform magnetic field, or proximity-couple to a ferromagnet, to generate a Zeeman term $H_z = J_z \tau_3 \sigma_3 \kappa_0$, where J_z is directly proportional to the magnitude of the external magnetic field (we ignore any orbital effects of the magnetic field). This term qualitatively modifies the band structures of $h_{SC,5}$ and $h_{SC,6}$. From Figs. 3(c) and 4(c) we see that the presence of the Zeeman term gaps out the surface states completely

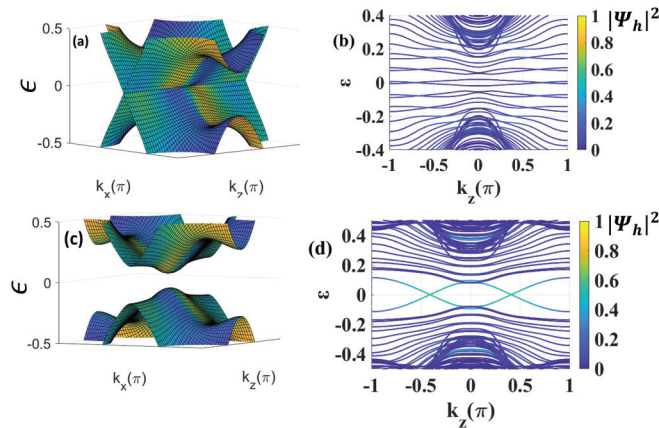


FIG. 4. Model $h_{SC,6}$: Surface states (a) in the k_x - k_z plane, and hinge states (b) along k_z , when $J_z = 0$, (c) and (d), same as (a) and (b), respectively, for the case when $J_z = 0.4$.

(it also gaps out the bulk nodes of $h_{SC,5}$). Furthermore, we see the appearance of clear hinge states within the gap of the surface states, as shown in Figs. 3(d) and 4(d). H_z breaks C_4 symmetry and both mirror symmetries, but leaves the products $C_4\mathcal{M}_x$ (antidiagonal mirror) and $C_4\mathcal{M}_y$ (diagonal mirror) intact. Because of these symmetries, and contrary to the hinge states of the other models discussed in this work, the hinge states of $h_{SC,5}$ and $h_{SC,6}$ (with Zeeman) are: dispersive, nonchiral, and localized only at two of the four hinges related by C_2 symmetry. In addition, we find that the pair of corners where the helical hinge states are localized switches upon a change of sign of the Zeeman term (e.g., switching the direction of the external magnetic field) (see Fig. 5). This phenomenon could be useful for the experimental detection of these systems. We note that magnetic fields were also proposed to induce a HOTSC state in a completely different system with different properties in two dimensions [35].

For $J_z > 0$ ($J_z < 0$) there are two, counterpropagating modes at two of the four corners, and they are \pm eigenstates of $C_4\mathcal{M}_y$ ($C_4\mathcal{M}_x$). The hinge modes are perturbatively stable even in the absence of the two $C_4\mathcal{M}_i$ symmetries as long as particle-hole symmetry is preserved. However, the modes can be destroyed through bulk or surface phase transitions. Because the hinge states are located at opposite sides of the antidiagonal (diagonal), the breaking of the $C_4\mathcal{M}_x$ ($C_4\mathcal{M}_y$) symmetry leads to nonsymmetric hinge states and, for a strong enough $C_4\mathcal{M}_x$ ($C_4\mathcal{M}_y$) symmetry-breaking perturbation, to the almost complete suppression of the hinge states at one corner and the enhancement of the hinge states at the opposite corner, as shown in Fig. 5(c).

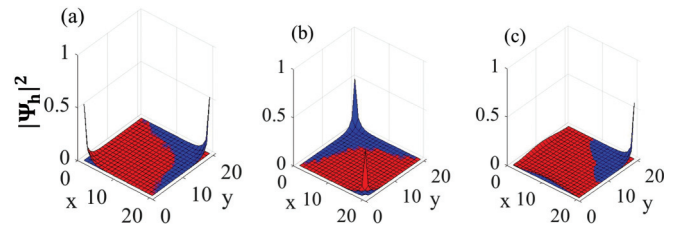


FIG. 5. $|\Psi_h(x, y)|^2$ for model $h_{SC,6}$ in the presence of a Zeeman term. We have two pairs of degenerate states. For each pair $|\Psi_h(x, y)|^2$ is the same. In the figure we show in blue and red the two different $|\Psi_h(x, y)|^2$ profiles. (a) $J_z = 0.4$, $k_z = 0.41\pi$, values for which the helical hinge bands cross [Fig. 4(d)]. (b) $J_z = -0.4$, $k_z = 0.41\pi$. (c) $J_z = 0.4$ plus $C_4\mathcal{M}_x$ breaking perturbation: $0.1\tau_3r_4^{-1}m_x$. In (c) $k_z = 0.19\pi$, for which we have the lowest positive energy.

In conclusion, we have identified a class of HOTSCs: *second-order Dirac superconductors*. HOTSCs in this class have both topologically protected Dirac cones for states at the surface (d-1 boundary) and topologically protected dispersionless Majorana states at the hinges (d-2 boundary). The coexistence of gapless surface and hinge modes should lead to novel transport properties that would be interesting to compare to those of conventional topological superconductors [2,36–46]. We have then identified 3D superconducting systems that can be driven into a higher-order topological state simply via inclusion of a Zeeman term, having dispersive helical Majorana hinge states that are located at only two (or one) of the corners. We have shown that by varying the relative sign of the Zeeman term and of the mirror-diagonal symmetry-breaking perturbation, the position of the Majorana pairs can be tuned to be at a specific corner, leading to a highly tunable setup for realizing, and detecting, helical Majorana states.

S.A.A.G., X.H., and E.R. acknowledge support from ARO (Grant No. W911NF-18-1-0290), NSF (Grant No. DMR-1455233-CAREER), and ONR (Grant No. ONR-N00014-16-1-3158). E.R. thanks the Aspen Center for Physics, which is supported by National Science Foundation Grant No. PHY-1607611, for its hospitality during the early stages of the work. The numerical calculations have been performed on computing facilities at William & Mary which were provided by contributions from the NSF, the Commonwealth of Virginia Equipment Trust Fund, and ONR. T.L.H. thanks the U.S. National Science Foundation under Grant No. DMR 1351895-CAR, and the MRSEC program under NSF Award No. DMR-1720633 (SuperSEED) for support.

- [1] R. Resta, *Rev. Mod. Phys.* **66**, 899 (1994).
 [2] C.-K. Chiu, J. C. Y. Teo, A. P. Schnyder, and S. Ryu, *Rev. Mod. Phys.* **88**, 035005 (2016).
 [3] J. Zak, *Phys. Rev. Lett.* **62**, 2747 (1989).
 [4] T. L. Hughes, E. Prodan, and B. A. Bernevig, *Phys. Rev. B* **83**, 245132 (2011).

- [5] A. M. Turner, Y. Zhang, R. S. K. Mong, and A. Vishwanath, *Phys. Rev. B* **85**, 165120 (2012).
 [6] W. A. Benalcazar, B. A. Bernevig, and T. L. Hughes, *Science* **357**, 61 (2017).
 [7] W. A. Benalcazar, B. A. Bernevig, and T. L. Hughes, *Phys. Rev. B* **96**, 245115 (2017).

- [8] F. Schindler, A. M. Cook, M. G. Vergniory, Z. Wang, S. S. P. Parkin, B. A. Bernevig, and T. Neupert, *Sci. Adv.* **4**, eaat0346 (2018).
- [9] Z. Song, Z. Fang, and C. Fang, *Phys. Rev. Lett.* **119**, 246402 (2017).
- [10] F. Schindler, Z. Wang, M. G. Vergniory, A. M. Cook, A. Murani, S. Sengupta, A. Y. Kasumov, R. Deblock, S. Jeon, I. Drozdov, H. Bouchiat, S. Guéron, A. Yazdani, B. A. Bernevig, and T. Neupert, *Nat. Phys.* **14**, 918 (2018).
- [11] M. Ezawa, *Phys. Rev. Lett.* **120**, 026801 (2018).
- [12] M. Ezawa, *Phys. Rev. B* **98**, 045125 (2018).
- [13] J. Noh, W. A. Benalcazar, S. Huang, M. J. Collins, K. P. Chen, T. L. Hughes, and M. C. Rechtsman, *Nat. Photonics* **12**, 408 (2018).
- [14] C. W. Peterson, W. A. Benalcazar, T. L. Hughes, and G. Bahl, *Nature (London)* **555**, 346 (2018).
- [15] S. Imhof, C. Berger, F. Bayer, J. Brehm, L. W. Molenkamp, T. Kiessling, F. Schindler, C. H. Lee, M. Greiter, T. Neupert, and R. Thomale, *Nat. Phys.* **14**, 925 (2018).
- [16] M. Serra-Garcia, V. Peri, R. Süssstrunk, O. R. Bilal, T. Larsen, L. G. Villanueva, and S. D. Huber, *Nature (London)* **555**, 342 (2018).
- [17] M. Ezawa, *Sci. Rep.* **9**, 5286 (2019).
- [18] J. Langbehn, Y. Peng, L. Trifunovic, F. von Oppen, and P. W. Brouwer, *Phys. Rev. Lett.* **119**, 246401 (2017).
- [19] Y. Wang, M. Lin, and T. L. Hughes, *Phys. Rev. B* **98**, 165144 (2018).
- [20] E. Khalaf, *Phys. Rev. B* **97**, 205136 (2018).
- [21] D. Călugăru, V. Juričić, and B. Roy, *Phys. Rev. B* **99**, 041301(R) (2019).
- [22] Z. Wang, B. J. Wieder, J. Li, B. Yan, and B. A. Bernevig, [arXiv:1806.11116](https://arxiv.org/abs/1806.11116).
- [23] B. J. Wieder and B. A. Bernevig, [arXiv:1810.02373](https://arxiv.org/abs/1810.02373).
- [24] W. A. Benalcazar, T. Li, and T. H. Hughes, *Phys. Rev. B* **99**, 245151 (2019).
- [25] B. J. Wieder, Z. Wang, J. Cano, X. Dai, L. M. Schoop, B. Bradlyn, and B. A. Bernevig (unpublished).
- [26] R.-X. Zhang, W. S. Cole, and S. Das Sarma, *Phys. Rev. Lett.* **122**, 187001 (2019).
- [27] Q. Wang, C.-C. Liu, Y.-M. Lu, and F. Zhang, *Phys. Rev. Lett.* **121**, 186801 (2018).
- [28] Z. Yan, F. Song, and Z. Wang, *Phys. Rev. Lett.* **121**, 096803 (2018).
- [29] C.-H. Hsu, P. Stano, J. Klinovaja, and D. Loss, *Phys. Rev. Lett.* **121**, 196801 (2018).
- [30] Y. Volpez, D. Loss, and J. Klinovaja, *Phys. Rev. Lett.* **122**, 126402 (2019).
- [31] Y.-J. Wu, J. Hou, Y.-M. Li, X.-W. Luo, and C. Zhang, [arXiv:1905.08896](https://arxiv.org/abs/1905.08896).
- [32] M. Lin and T. L. Hughes, *Phys. Rev. B* **98**, 241103(R) (2018).
- [33] T. Hashimoto, S. Kobayashi, Y. Tanaka, and M. Sato, *Phys. Rev. B* **94**, 014510 (2016).
- [34] See Supplemental Material at <http://link.aps.org/supplemental/10.1103/PhysRevB.100.020509> for details on bulk bandstructures, discussion of model $h_{SC,(2)}$, the effect of perturbations on $h_{SC,(1,2)}$ and the calculation of quadrupolelike moment for model $h_{SC,1}$.
- [35] X. Zhu, *Phys. Rev. B* **97**, 205134 (2018).
- [36] L. Fu and C. L. Kane, *Phys. Rev. Lett.* **102**, 216403 (2009).
- [37] L. Fu and C. L. Kane, *Phys. Rev. B* **79**, 161408(R) (2009).
- [38] M. S. Foster and E. A. Yuzbashyan, *Phys. Rev. Lett.* **109**, 246801 (2012).
- [39] M. S. Foster, H.-Y. Xie, and Y.-Z. Chou, *Phys. Rev. B* **89**, 155140 (2014).
- [40] Sayed Ali Akbar Ghorashi, S. Davis, and M. S. Foster, *Phys. Rev. B* **95**, 144503 (2017).
- [41] Sayed Ali Akbar Ghorashi, Y. Liao, and M. S. Foster, *Phys. Rev. Lett.* **121**, 016802 (2018).
- [42] B. Roy, Sayed Ali Akbar Ghorashi, M. S. Foster, and A. H. Nevidomskyy, *Phys. Rev. B* **99**, 054505 (2019).
- [43] Sayed Ali Akbar Ghorashi and M. S. Foster, [arXiv:1903.11086](https://arxiv.org/abs/1903.11086).
- [44] H.-Y. Xie, Y.-Z. Chou, and M. S. Foster, *Phys. Rev. B* **91**, 024203 (2015).
- [45] S. A. Yang, H. Pan, and F. Zhang, *Phys. Rev. Lett.* **113**, 046401 (2014).
- [46] H. Hu, F. Zhang, and C. Zhang, *Phys. Rev. Lett.* **121**, 185302 (2018).